Vapor Recompression for Efficient Distillation. 1. A New Synthesis Perspective on Standard Configurations

N. Felbab
Centre of Material and Process Synthesis, School of Chemical and Metallurgical Engineering, University of the Witwatersrand, Johannesburg, South Africa

B. Patel
Centre of Material and Process Synthesis, School of Chemical and Metallurgical Engineering, University of the Witwatersrand, Johannesburg, South Africa

Dept. of Civil and Chemical Engineering, University of South Africa, Pretoria, South Africa

M. M. El-Halwagi
Dept. of Chemical Engineering, Texas A&M University, College Station, TX 77843

Dept. of Chemical and Materials Engineering, King Abdulaziz University, Jeddah, Saudi Arabia

D. Hildebrandt and D. Glasser
Centre of Material and Process Synthesis, School of Chemical and Metallurgical Engineering, University of the Witwatersrand, Johannesburg, South Africa

DOI 10.1002/aic.14070
Published online March 20, 2013 in Wiley Online Library (wileyonlinelibrary.com)

The vapor recompression (VRC) distillation scheme is examined and compared with conventional distillation in an analysis spanning fundamental thermodynamics, high-level calculations, and rigorous simulation. The purpose of this article is three-fold: first, it provides greater insight into VRC distillation. Second, it provides a process synthesis tool to rapidly assess whether VRC is likely to be more thermodynamically favorable than conventional distillation for a given split. Third, it may be used to determine if VRC can be implemented practically. The tool presented in the article is consolidated in the form of a single chart, for which only the top and bottom product temperatures are required to determine the outcome. Using this chart, first-pass estimates can be obtained with no calculations whatsoever. The tool, which appears to be the first of its kind in this context, is validated with examples and rigorous simulation. © 2013 American Institute of Chemical Engineers *AIChE J*, 59: 2977–2992, 2013
Keywords: distillation, energy, process synthesis, thermodynamics/classical

Introduction

Despite the well-established fact that distillation is an energetically inefficient process,[1–3] it has seen widespread industrial application for the separation of mixtures over the last century: by Humphrey's[4] estimate, up to 90% of all product recovery. Conventional, or simple, distillation columns (those with one feed, a distillate, a bottoms, a condenser, and a reboiler; see Figure 1a) are the most prevalent, even though they are often not the most efficient distillation configuration.

Improvements in the energy efficiency of distillation remain a challenge for industry, especially due to the rising costs of energy and growing environmental concerns. In an attempt to mitigate this, a large number of increasingly complex modifications to, and departures from, conventional distillation have been devised over the last few decades. These include:

1. Complex distillation arrangements/column coupling[5–10] (e.g., Petlyuk,[11–14] multieffect,[15–17] and distributed-feed columns[18–20]);
2. Diabatic columns[21,22] (in which heat is added or removed on several or all stages, allowing the column to operate more reversibly);
3. Heat-pumping techniques[23] (e.g., vapor recompression (VRC) and absorption heat pumps);
4. Heat-integrated distillation columns[24–30] (in which the rectifying section is compressed and transfers heat to the stripping section, using a combination of the first three modifications).

The literature covering these topics is vast (which is indicative of the urgency to find energy savings in distillation processes); thorough reviews and comparisons can be found in Rév et al.,[5] Nakaiwa et al.,[31] and Jana.[32]

Research related to energy-efficient columns is on a trajectory of increasing complexity, with simpler systems thought to be well-understood. One such class of "simple" systems is heat-pump-assisted distillation, of which there are three typically used variants: VRC; the closed-cycle process, which

Correspondence concerning this article should be addressed to N. Felbab at Nik.Felbab@gmail.com.

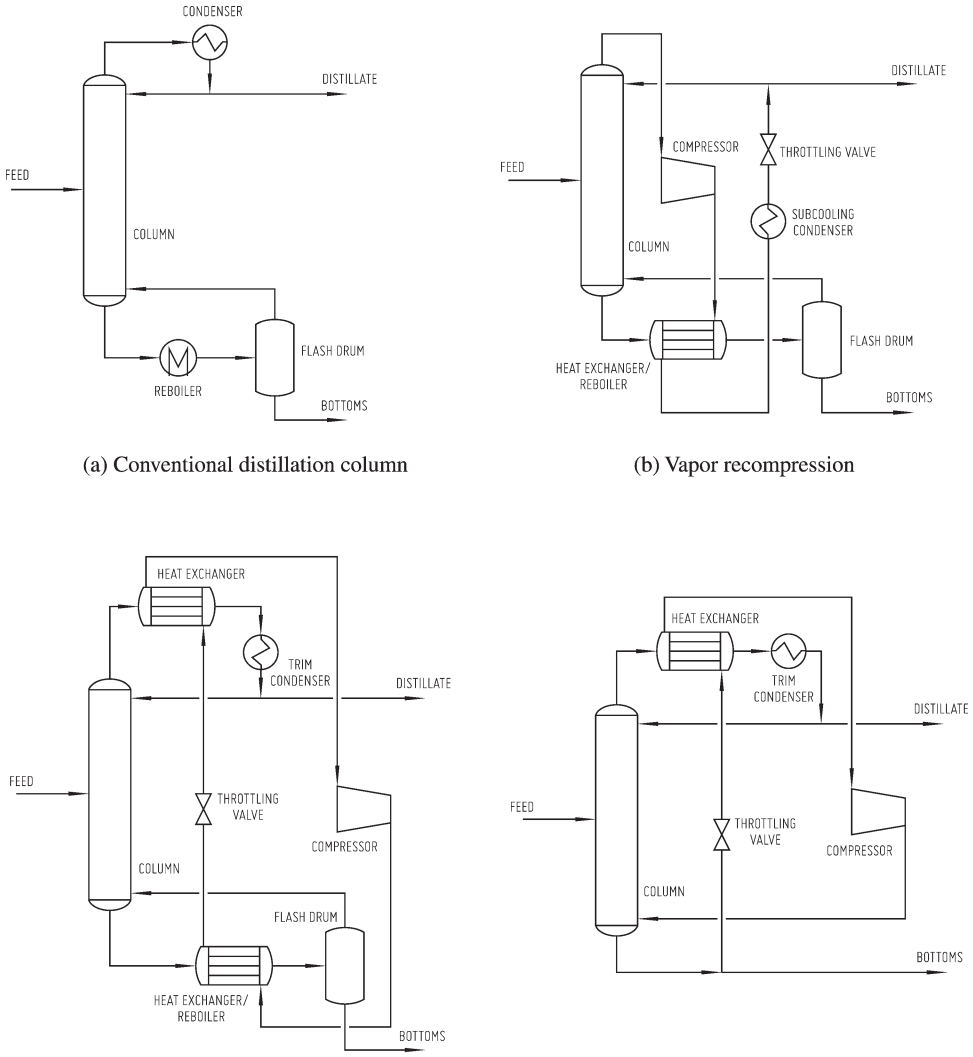

(a) Conventional distillation column

(b) Vapor recompression

(c) Heat pump with external working fluid

(d) Bottoms flashing

Figure 1. Schematic representations of (a) conventional distillation, and (b–d) the three most common heat-pump-assisted distillation configurations.

involves the use of an external working fluid; and bottoms flashing.[33–36] Figures 1b–d show the general schematics of these configurations, respectively. Of these three alternatives, VRC has been found to be the most advantageous and economical.[23,37,38]

The application of VRC to distillation has been studied extensively.[23,33,35,37–46] The literature to date has focused mainly on the detailed analysis and simulation of various systems, on the economic optimization of these systems and their operating conditions, and on controllability. Many of these studies have found—for the various systems studied—that VRC is most beneficial for close-boiling mixtures, systems which require high heat loads, small column pressure drops, and low process temperatures.[41,47]

Previous research has dealt with simulation or optimization of standard VRC (SVRC), but has not considered a generalized process synthesis approach. It is this gap in the literature that this article is aiming to bridge; the main goal of this article is to develop a tool that can rapidly provide insight into the operation of SVRC prior to rigorous simulation. This tool can assess whether or not SVRC is inherently more efficient for a given split than conventional distillation at the most fundamental thermodynamic level, and whether or not it is likely that SVRC could be implemented practically. In this way, rigorous calculation, simulation, and optimization effort—which can be substantial—need not be wasted if there is no possible benefit to using SVRC for a given problem. The presented methodology can be used to discard clearly unfavorable alternatives immediately; unlike optimization, its purpose is not to find the best possible alternative.

Previously, thermodynamic analyses using the first[1–3] and second[6,21,22,48–51] laws have been performed on conventional distillation columns. A review of the application of thermodynamic analyses to separation systems—and conventional distillation in particular—can found in Demirel.[36]

In this article, fundamental thermodynamic principles are applied to SVRC. The main innovation of this work is the presentation of the resulting process synthesis tool as a single chart (see Figure 10), for which only the distillate and bottoms temperatures are required. Using solely these two temperatures, estimates can be made of whether or not SVRC is inherently thermodynamically more efficient than conventional distillation, and the minimum compression ratio (a technical deciding factor for practical implementation) can be determined. Moreover, if the ideal gas heat capacity of the overhead vapor is known, it is possible to estimate

whether superheating of the compressor inlet is necessary to avoid condensation on compression. Using this tool, the applicability of VRC can be assessed completely graphically; that is, with no calculations at all. This appears to be the first approach of its kind for SVRC; previously, no general guidelines for rapidly determining if VRC is worthwhile have been presented in the open scientific literature. In this era, in which energy savings are becoming more and more crucial, it is useful to have simple guidelines to aid the engineer in the decision-making process; this applies equally to greenfield projects and to retrofitting.

In the sections that follow, a thermodynamic analysis of conventional columns is first presented. This then provides a basis for comparison with SVRC, which considers energy flows, as well as work flows. Thereafter, a general thermodynamic criterion for the rapid determination of the efficiency of SVRC compared to conventional distillation is presented. Additional indicators for two key variables—compression ratio and compressor inlet superheating—are incorporated; these dictate whether or not it might be possible to implement the SVRC practically. All of this information is consolidated in Figure 10, which allows for entirely graphical estimation of whether or not SVRC is likely to be favorable and feasible for a given problem. The results are confirmed with a number of rigorous simulations.

Throughout this work, ambient pressure (P_0) and temperature (T_0) are taken to be 101 325 Pa and 298.15 K, respectively. As the thermodynamic basis, pure liquids are taken to have zero enthalpy and entropy at ambient conditions. Vapors are treated as ideal gases, since the pressures used in VRC are sufficiently low to make effects of nonideality negligible. As a convention, component indices in a mixture are arranged in order of volatility, with "1" being the most volatile, for example $x_{F,2}$ refers to the liquid mole fraction of the second-lightest component in the feed.

Simplifying Assumptions

The rigorous simulation and comparison of conventional columns and SVRC can be a time-consuming endeavor, and a potentially wasted one if SVRC proves not to be advantageous or even technically feasible. To reduce this wasted effort, the main aim of this work is to derive a tool that gives a preliminary indication as to whether SVRC might have benefits over conventional distillation; rigorous simulation is then only undertaken when this preliminary indication shows evidence of potential benefits. With this goal in mind, it is clear that the synthesis tool should be fast, simple, and analytical (as opposed to computational). For the purposes of arriving at simple, high-level calculations for easy analysis, a number of assumptions are made in this article:

1. The reboiler adds work as a reversible heat pump, and the condenser removes work as a reversible heat engine. As will be seen later, the purpose of the thermodynamic analysis in this article is to compare the best inherent performance of the conventional and SVRC configurations; this reversibility represents the limit of operation for these pieces of equipment, and is, thus, an appropriate assumption;

2. The feed and products are liquid. This is a common scenario in distillation, and here it serves the purpose of removing a degree of freedom, thereby reducing the number of variables to one amenable to high-level analysis;

3. The feed mixture is a binary, ideal mixture. The fact that it is binary allows for pure-component products in the configurations considered in this article (see the next point). Its ideality removes the complexity associated with nonideal mixtures, which would require iterative computations, and would, thus, render the analytical equations derived in this article impossible; instead, the simple constant relative volatility model can be used;

4. The feed mixture is split into pure components, with the pure light component recovered in the distillate, and the pure heavy component recovered in the bottoms. The purpose of this complete separation is three-fold: first, it represents the limit of operation in terms of degree of separation, and is also a reasonable approximation of the most typical separation problems, in which quite pure products are sought; second, it removes degrees of freedom, and allows the analysis to focus on more important variables; and finally, it allows for easier analysis, because the product vapor and liquid saturation temperatures are simply the pure-component boiling points, eliminating the need for iterative bubble- or dew-point calculations, and additional property information;

5. The distillation column adheres to constant molar overflow (CMO): sensible heat effects are negligible in comparison with latent heat, heat of mixing is zero, all components have the same latent heat, and the column is adiabatic. This is a very common simplification that is generally quite accurate for ideal and near-ideal mixtures.

The examples presented later in the section "Rigorous Simulation and Validation" each deviate from one or more of the above assumptions, and it would appear that the applicability of the proposed approach does not diminish appreciably as a result of these simplifying assumptions. Note that the assumption of a binary mixture in point 3, and of pure-component products in point 4 above, are not strictly necessary for the novel methodology proposed in this article, as long as the product temperatures are known; these assumptions merely simplify the analysis in this article.

Thermodynamic Analysis: Conventional Distillation Columns

In this section, a brief, high-level thermodynamic analysis of conventional distillation is performed. The foundation of this work is well-known,[52–56] but it is included here to serve as a basis for comparison with the SVRC scheme.

Conventional distillation columns can be thought of as a coupled heat pump and heat engine, where the former adds work to the column (reboiler), and the latter removes it (condenser). The input work is greater than the output work, such that there is net addition of work to the column, part of which is used to perform the separation, and the remainder of which contributes to entropy generation. This is a well-established[57–60] understanding of the fundamental work flows in distillation columns: they extract work from heat flows by degrading the quality of the heat.

To improve overall process efficiency, the work flow that is removed from the column can, in some cases, be reused in another part of the process, as long as that part of the process can accept lower-quality heat.[61] This is the preferred approach; however, in the absence of the overall process context, this article will consider the distillation system in isolation.

Work addition and removal in distillation columns

Figure 2 shows a schematic representation of the work inputs and outputs, and also serves as a reference for the

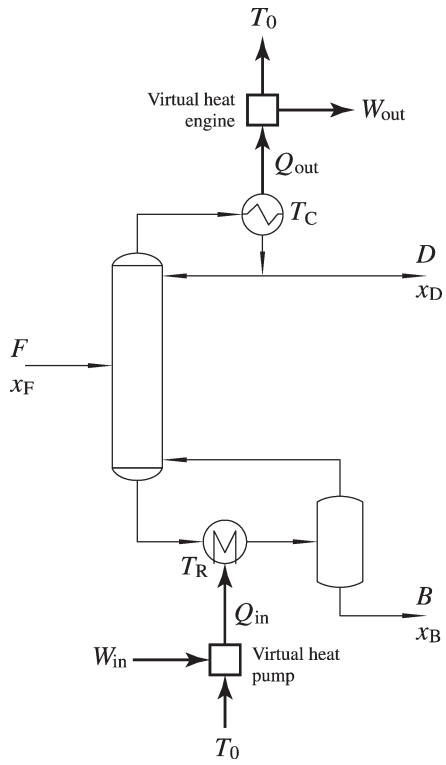

Figure 2. Schematic representation of a conventional distillation column, along with the mass, heat, and work flows in and out of the system, as well as the significant temperatures.

nomenclature used in this section. Assuming a reversible heat pump, the work input is expressed mathematically as

$$W_{in} = Q_{in}\left(1-\frac{T_0}{T_R}\right) \tag{1}$$

The work removed from the column by a reversible heat engine is

$$W_{out} = Q_{out}\left(1-\frac{T_0}{T_C}\right) \tag{2}$$

Minimum theoretical energy input to effect separation (reversible distillation model)

An entropy analysis over the column gives

$$F\hat{S}_F + \frac{Q_{in}}{T_R} + S_{gen} = D\hat{S}_D + B\hat{S}_B + \frac{Q_{out}}{T_C} \tag{3}$$

The temperatures of heat input and output are taken at the limit of performance; that is, countercurrent heat exchangers with infinite heat-transfer area are assumed, such that the heating medium enters at the temperature of the process stream outlet, and the cooling medium leaves at the process stream inlet temperature. In other words, heat is added at the process stream outlet temperature, and it is removed at the process stream inlet temperature.

A reversible column is one that generates no entropy, that is $S_{gen} = 0\,\mathrm{W/K}$. This is the ideal case, in that no work is wasted, and it demarcates the theoretical limit of performance: no distillation column could be more efficient than a completely reversible one. Consequently, a reversible column represents the minimum theoretical heat requirement of a distillation column to perform a given separation.

Assuming a column that generates no entropy ($S_{gen} = 0\,\mathrm{W/K}$), and separates the feed mixture into pure liquid components ($\hat{S}_D = \hat{S}_B = 0$), Eq. 3 becomes

$$F\Delta\hat{S}_{mix} + \frac{Q_{in}}{T_R} = \frac{Q_{out}}{T_C} \tag{4}$$

The assumptions made in this section also give an energy balance of $Q_{in} = Q_{out}$, hence

$$\Delta\hat{S}_{mix} = \frac{Q_{in}}{F}\left(\frac{1}{T_C}-\frac{1}{T_R}\right) \tag{5}$$

Rearranging Eq. 5 and recognizing that $\Delta\hat{S}_{mix} = -R\sum x_i \ln x_i$ for ideal mixtures, the following is obtained

$$Q_{in,sep} = -\frac{FR\sum x_{F,i}\ln x_{F,i}}{\frac{1}{T_C}-\frac{1}{T_R}} \tag{6}$$

Equation 6 represents the minimum theoretical heat input required to perform the separation.

Furthermore, Eq. 5 can be substituted into Eq. 1 to give

$$F\Delta\hat{S}_{mix} = \frac{W_{in,sep}}{T_C}\left(\frac{T_R-T_C}{T_R-T_0}\right) \tag{7}$$

The relationship in Eq. 7 will be useful later.

Minimum practical energy input

In practice, distillation columns have a minimum heat input that is different from Eq. 6 owing to their internal configuration, with the minimum heat requirement corresponding to minimum reflux. Using a simple derivation (which is given in Appendix A), with minimum reflux estimated by Underwood's method,[62] the following equation gives the minimum practical heat input into a distillation column

$$Q_{in,min} = F\lambda\left(\frac{1}{\alpha-1}+x_{F,1}\right) \tag{8}$$

Comparison of theoretical and practical minimum energy

It is now possible to compare the practical minimum heat input, Eq. 8, with the theoretical minimum, Eq. 6. To do this, Q_{in}/F for the practical and theoretical minima is plotted as a function of feed composition in Figure 3; the systems considered and their (constant) properties are given in Table 1. The chosen systems cover a wide range of relative volatilities (or differences in reboiler and condenser temperatures, which are related) to assess why some are amenable to VRC, and others not.

Figure 3 not only shows that the separation of wider-boiling mixtures requires less energy than that of narrow-boiling ones, but also that these mixtures can operate closer to their theoretical minima using the conventional distillation column. However, the most important insight that this figure offers is

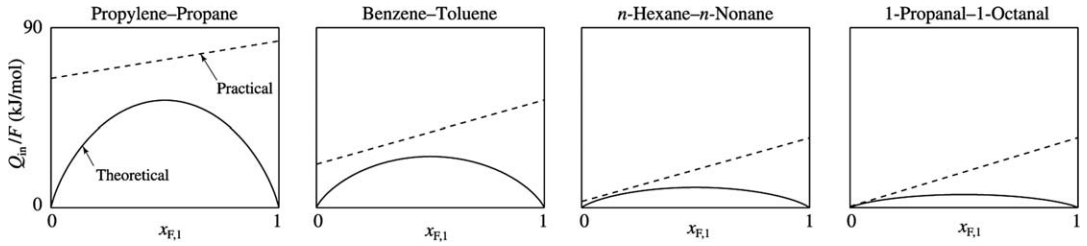

Figure 3. Comparison of minimum theoretical heat input and minimum practical heat input to a conventional distillation column for a sharp split as a function of mole fraction of the light component in the feed.

that conventional distillation becomes less and less efficient as the feed tends to higher purity in either direction. This is an intuitive result, because theoretically, little work addition is required to effect a small degree of separation. In reality, however, the operation of a distillation column requires vaporization in the reboiler, which does not necessarily contribute to the separation process itself; indeed, a feed with an infinitesimal amount of impurity requires effectively no work of separation, yet vaporization must still take place. This vaporization is not proportional to the degree of impurity in the feed.

Thermodynamic Analysis: SVRC Scheme

A simple diagram of the SVRC scheme is given in Figure 1b. Vapor leaving the top of the column is compressed isentropically, causing an increase in both pressure and temperature. The purpose of the compression is two-fold: first, it elevates the temperature of the overhead vapor to provide a driving force for heat transfer to the bottom liquid; second, it elevates the dew point of the overhead vapor, allowing its latent heat to be used at a higher temperature. This overhead vapor stream—the temperature of which exceeds that of the bottoms—is heat exchanged with the liquid leaving the bottom of the column, partially vaporizing the latter; in other words, the overhead vapor stream uses its latent heat to vaporize the liquid, and in the process, it itself condenses. This partially condensed stream is then subcooled in the condenser to such a point that when its pressure is dropped back down to the column pressure, it does not vaporize (ideally, it should be a saturated liquid). Part of this liquid stream is refluxed to the column, and the remainder is drawn off as the distillate. Overall, energy is only added to the compressor, and it is removed in the condenser.

Figure 4 shows a schematic representation of the mass and energy flows in the SVRC configuration; it also provides stream labels for the important streams. Table 2 gives the relationship of T, P, and phase for these streams, assuming complete separation of the binary feed. To aid understanding further, a qualitative pressure–enthalpy plot relating to the process is given in Figure 5. Note that while Figure 1b does not include a superheater prior to compression, Figure 4 does, because some saturated vapors condense on isentropic compression, which must strictly be avoided in a compressor.[45,63,64] This is discussed at greater length later in this section.

Minimum theoretical energy input to effect separation in SVRC (reversible model)

The use of the superheater may be necessary for some fluids, but will be disregarded for the present, high-level analysis, that is $Q_{sh} = 0\,\mathrm{W}$, as it is not a set feature of SVRC. Using the same assumptions as before, the energy balance around the system reduces to

$$W_{comp} = Q_{out} \tag{9}$$

The compression is performed isentropically, which, by definition, means that the compression step itself generates no entropy. As in the case of the conventional distillation model, heat is removed at the temperature of the process stream inlet to the heat exchanger, which in this case is T_4. Consequently, the entropy analysis (assuming reversibility) is

$$F\Delta\hat{S}_{mix} = \frac{Q_{out}}{T_4} \tag{10}$$

On substitution of Eq. 9 into Eq. 10, the following relationship is obtained

$$F\Delta\hat{S}_{mix} = \frac{W_{comp}}{T_4} \tag{11}$$

The left-hand side of Eq. 11 is fixed by the problem specification, but the value of T_4 is less obvious. Indeed, T_4 can be manipulated using different design parameters. To provide a driving force for the heat exchange $T_4 > T_R$; however, the limit of operation occurs in a heat exchanger with infinite heat exchange area, in which case $T_4 = T_R$. The latter also minimizes W_{comp} according to Eq. 11. Consequently, the following interpretation is used

$$F\Delta\hat{S}_{mix} = \frac{W_{comp}}{T_R} \tag{12}$$

Table 1. Binary Systems and Simple Constant Properties Used in High-Level Calculations

No.	Light (1)	Heavy (2)	α	λ (kJ/mol)	$\hat{C}_{p,1}^{IG}$ (J/mol·K)	T_C (K)	T_R (K)
1	Propylene	Propane	1.29	18.73	53.4	225.5	231.1
2	Acetonitrile	Nitromethane	1.84	32.32	58.3	354.8	374.4
3	Benzene	Toluene	2.47	31.98	104.9	353.3	383.8
4	*n*-Hexane	*n*-Nonane	11.21	31.84	175.6	341.9	424.0
5	1-Propanal	1-Octanal	58.47	34.46	174.1	321.1	447.3

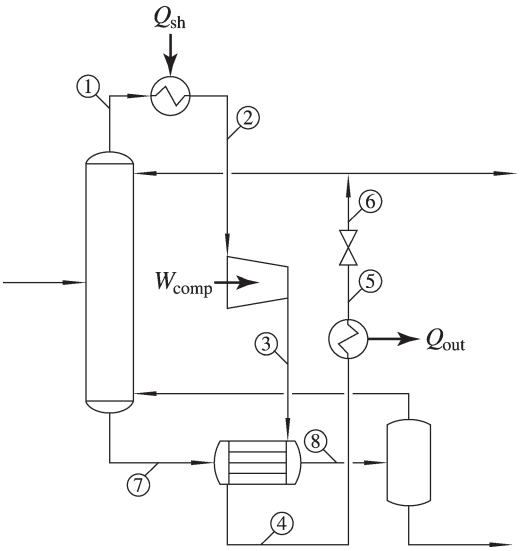

Figure 4. Schematic representation of the SVRC configuration, with stream labels.

See Table 2 for stream information.

The minimum theoretical energy (and work) addition using a perfect compressor, therefore, is given by

$$W_{\text{comp, sep}} = T_{\text{R}} F \Delta \hat{S}_{\text{mix}} \tag{13}$$

$$W_{\text{comp, sep}} = -FRT_{\text{R}} \sum x_{\text{F},i} \ln x_{\text{F},i} \tag{14}$$

Minimum practical energy input in SVRC

As with the conventional column, the mass balance and minimum reflux ratio impose limitations on the minimum energy that is practically required to operate the SVRC configuration. In this section, an idealized SVRC model is derived, but with the inclusion of fundamental mass balance constraints that are inherent to the operation of distillation columns.

An important point to take into consideration is that the saturated vapors of some fluids become superheated on isentropic compression, while others condense. The following criterion can determine which of those two outcomes occurs[65]

$$\begin{aligned} \hat{C}_{p,1}^{\text{IG}} T_{\text{C}} &< \lambda \,(\text{superheated}) \\ \hat{C}_{p,1}^{\text{IG}} T_{\text{C}} &> \lambda \,(\text{partially condensed}) \end{aligned} \tag{15}$$

Table 2. Relationship of Temperature, Pressure, and Phase in Streams in Figure 4, Assuming Complete Separation of the Binary Feed

Stream	T	P	Phase
1	T_{C}	P_0	Saturated vapor
2	$T_2 (>T_{\text{C}})$	P_0	Superheated vapor
3	$T_3 (>T_2)$	P_{comp}	Superheated or saturated vapor
4	$T_4 (>T_{\text{R}})$	P_{comp}	Saturated vapor and liquid
5	T_{C}	P_{comp}	Subcooled liquid
6	T_{C}	P_0	Saturated liquid
7	T_{R}	P_0	Saturated liquid
8	T_{R}	P_0	Saturated vapor and liquid

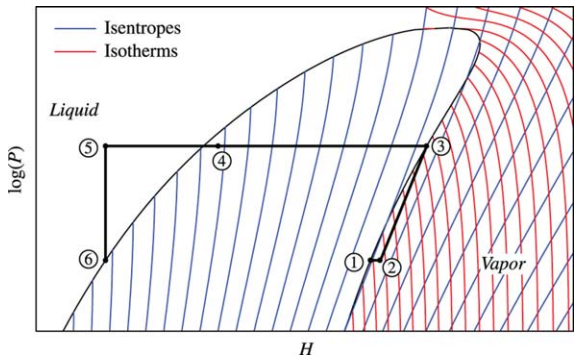

Figure 5. Qualitative pressure–enthalpy plot showing the vapor recompression process relating to Figure 4, and assuming minimum compressor inlet superheating.

[Color figure can be viewed in the online issue, which is available at wileyonlinelibrary.com]

Besides the practical issue of liquid formation in the condenser, if some of the fluid condenses within the compressor, the stream's full latent heat is not available to perform the reboil duty. If the fluid condenses, a superheater is used prior to compression to avoid condensation. Figure 6 best illustrates the P–T behavior in these instances, and the application of superheating. Minimum superheating results in a saturated vapor at the compressor outlet.

In either case, the pressure must be raised to a point where the condensing temperature is greater than T_{R}, or, in the limit, equal to T_{R}. Because the minimum energy input is sought in this section, this limit will be used.

If the saturated vapor superheats on compression, then, as derived in Appendix A, the energy/work input in the compressor is given by

$$W_{\text{comp, min}} = F\hat{C}_{p,1}^{\text{IG}} T_{\text{C}} \left(\frac{1}{\alpha - 1} + x_{\text{F},1} \right) \left[\exp\left(\frac{\lambda}{\hat{C}_{p,1}^{\text{IG}}} \left(\frac{1}{T_{\text{C}}} - \frac{1}{T_{\text{R}}} \right) \right) - 1 \right] \tag{16}$$

The total energy (and work) input into the system in this case is simply equal to $W_{\text{comp, min}}$.

If the saturated vapor condenses, then superheating is required. The minimum energy input to the superheater is, as shown in Appendix A

$$Q_{\text{sh, min}} = F\hat{C}_{p,1}^{\text{IG}} \left(\frac{1}{\alpha - 1} + x_{\text{F},1} \right) \left[T_{\text{R}} \exp\left(\frac{\lambda}{\hat{C}_{p,1}^{\text{IG}}} \left(\frac{1}{T_{\text{R}}} - \frac{1}{T_{\text{C}}} \right) \right) - T_{\text{C}} \right] \tag{17}$$

After the superheater, compression takes place, the energy input of which is given by the following

$$W_{\text{comp, min}} = F\hat{C}_{p,1}^{\text{IG}} T_{\text{R}} \left(\frac{1}{\alpha - 1} + x_{\text{F},1} \right) \left[1 - \exp\left(\frac{\lambda}{\hat{C}_{p,1}^{\text{IG}}} \left(\frac{1}{T_{\text{R}}} - \frac{1}{T_{\text{C}}} \right) \right) \right] \tag{18}$$

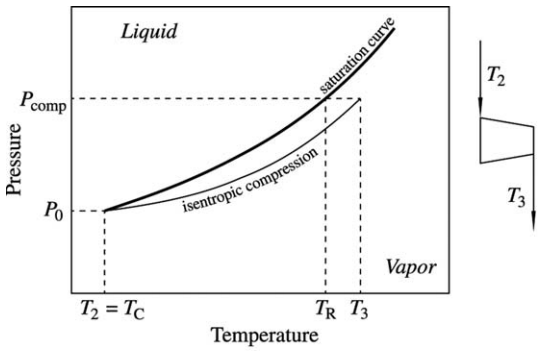

(a) Fluid that superheats on isentropic compression

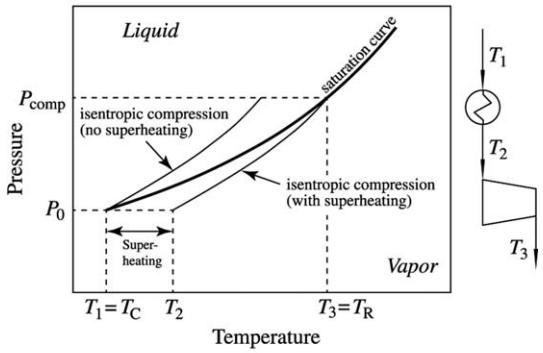

(b) Fluid that condenses on isentropic compression

Figure 6. Pressure–temperature behavior of a saturated vapor that (a) superheats on compression and (b) condenses on compression and requires superheating.

Note that the isentropic compression curves assume vapor compression; if this line enters the liquid region, that assumption is incorrect, and some liquid is formed, in which case, the true compression profile simply follows the saturation curve.

The derivation for Eq. 18 is given in Appendix A. In the case of the saturated vapor condensing on compression, the total energy input into the system is the sum of Eqs. 17 and 18.

Comparison of theoretical and practical minimum energy input

Using the above equations, it is possible to compare the minimum theoretical energy input—Eq. 14—with the practical minimum, for the same systems as in Figure 3. For saturated vapors that superheat on isentropic compression, the minimum practical energy input is given by Eq. 16; for fluids that condense, it is the sum of Eqs. 17 and 18. This comparison is shown in Figure 7, with the minimum compression ratios indicated for each system.

Note that the range of the y axis is much smaller in Figure 7 than in Figure 3. This illustrates that SVRC is more energy-efficient in all of the examined systems, even when compressor inlet superheating is required. (There is a cross-over point with very wide-boiling systems, for which conventional distillation is more efficient than SVRC; this is examined later.)

It is also noteworthy that the observed trend using SVRC is the opposite of that in conventional columns: wider-boiling mixtures require more energy to separate fully, and cannot operate as close to the theoretical minimum as close-boiling separations can.

Comparison of Work Inputs in Conventional and SVRC Distillation

When comparing the same process with different parameters, as has been done above, energy is a sufficient indicator of efficiency. However, the comparison of work input into different processes is more instructive than energy input, as it correlates with actual resource consumption (coal, natural gas, etc.), and takes the quality of heat into account. For example, a process could require a large heat load that needs to be supplied at ambient temperature, in which case that energy is effectively "free"; a process with a smaller heat load that requires heat at 800 K would need to consume resources to obtain that high-quality heat.

The equations for work input can be deduced easily.

Minimum theoretical work input in conventional distillation columns

$\Delta\hat{S}_{mix} = -R\sum x_i \ln x_i$ can be substituted into Eq. 7 and the result rearranged to obtain the minimum theoretical work input into a conventional distillation column

$$W_{in,sep} = -FRT_C\left(\frac{T_R - T_0}{T_R - T_C}\right)\sum x_{F,i}\ln x_{F,i} \tag{19}$$

Minimum practical work input in conventional distillation columns

The practical minimum work input is found by substituting Eq. 8 into Eq. 1 to obtain

$$W_{in,min} = F\lambda\left(\frac{1}{\alpha - 1} + x_{F,1}\right)\left(1 - \frac{T_0}{T_R}\right) \tag{20}$$

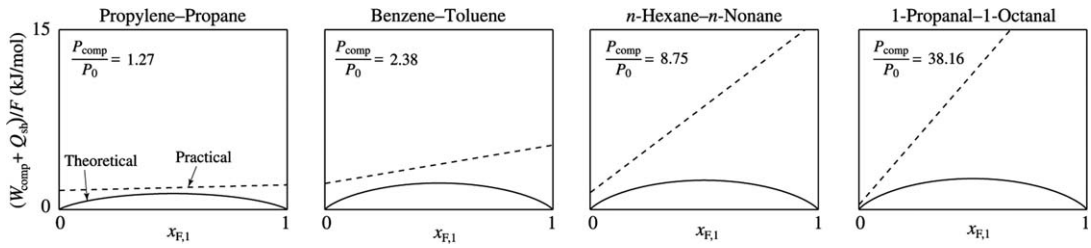

Figure 7. Comparison of minimum theoretical and minimum practical energy inputs to the standard vapor recompression configuration for a sharp split as a function of mole fraction of the light component in the feed.

The minimum compression ratios are indicated.

Minimum theoretical work input in SVRC

In the SVRC scheme, the energy and work inputs in the compressor are equivalent. Therefore, the minimum theoretical work input into the SVRC—assuming no compressor inlet superheating—is given by Eq. 14.

Minimum practical work input in SVRC

For the SVRC when no superheating is necessary, the practical minimum work input is given by Eq. 16.

If compressor superheating is necessary, the virtual work associated with the heat in the superheater is obtained by substituting Eq. 17 into Eq. 1, noting that the heat is added not at T_R but at T_2 (the expression for which is given in Appendix A)

$$W_{\text{sh, min}} = F\hat{C}_{p,1}^{\text{IG}}\left(\frac{1}{\alpha-1}+x_{\text{F},1}\right)\left[T_R\exp\left(\frac{\lambda}{\hat{C}_{p,1}^{\text{IG}}}\left(\frac{1}{T_R}-\frac{1}{T_C}\right)\right)-T_C\right]\left[1-\frac{T_0}{T_R}\exp\left(\frac{\lambda}{\hat{C}_{p,1}^{\text{IG}}}\left(\frac{1}{T_C}-\frac{1}{T_R}\right)\right)\right] \tag{21}$$

In this case, the work input in the compressor is simply Eq. 18, such that the total work input, when superheating is required, is the sum of Eqs. 21 and 18.

Using the above equations, plots of the minimum theoretical and practical work inputs for conventional and SVRC distillation as a function of feed composition are made in Figure 8. The same mixtures as in Figures 3 and 7 are used, with the exception of the propylene–propane system, which has normal boiling points below ambient temperature and, thus, requires elevated pressures or a refrigeration system.

Figure 8 shows that the scale of work input into the two configurations is much more comparable than that of energy input. This can largely be attributed to the fact that the energy input in a compressor is "pure" work, while only a temperature-dependent fraction of heat input is virtual work, in accordance with Eq. 1. The qualitative behavior of minimum theoretical and practical work as a function of feed composition is the same as with energy input. In systems with small temperature differences between the distillate and bottoms, the expected result is seen: SVRC is better than conventional distillation. However, there is a cross-over point, where the work input in the two cases is equivalent (see, e.g., the *n*-hexane–*n*-nonane split, where the two configurations are nearly the same). For wide-boiling mixtures, such as 1-propanal–1-octanal, the SVRC is worse than conventional distillation.

A quantitative description of this cross-over point is derived in the next section.

Thermodynamic and Practical Synthesis Targets

For a fixed feed, $F\Delta\hat{S}_{\text{mix}}$ is fixed, and is the same in the conventional distillation case, Eq. 7, and in the SVRC case, Eq. 12. Thus, $F\Delta\hat{S}_{\text{mix}}$ in the two cases can be equated to obtain

$$\frac{W_{\text{in}}}{T_C}\left(\frac{T_R-T_C}{T_R-T_0}\right)=\frac{W_{\text{comp}}}{T_R} \tag{22}$$

To find the region where SVRC is better than conventional distillation, a boundary must be defined where the work input in the two cases is the same, that is, $W_{\text{in}}=W_{\text{comp}}$. Applying this to Eq. 22 and rearranging the result leads to the following equation

$$T_C=\frac{T_R^2}{2T_R-T_0} \tag{23}$$

Equation 23 describes the relationship between T_R and T_C where the work input into the conventional column and SVRC configuration is the same, at a fundamental thermodynamic level.

Figure 9 shows a plot that demarcates the region where SVRC is more thermodynamically efficient than conventional distillation as a function of the reboiler and condenser temperatures (boiling points of the feed mixture's constituent components, in the sharp-split case).

Although this article focuses on SVRC, the same analysis can be performed on the other configurations in Figure 1, that is, heat-pump-assisted distillation with an external working fluid, and bottoms flashing. A brief analysis of these configurations can be found in Appendix B.

Compression ratios

Despite the fact that the SVRC region in Figure 9 is quite large, VRC is used relatively seldom. This can be explained by the practical consideration mentioned earlier: large differences between T_C and T_R require a large increase in temperature in the compressor, which in turn translates to a high compression ratio. Compressors with high compression ratios are uneconomical and inefficient. Consequently, it is useful to represent this practical limitation alongside the fundamental thermodynamic one.

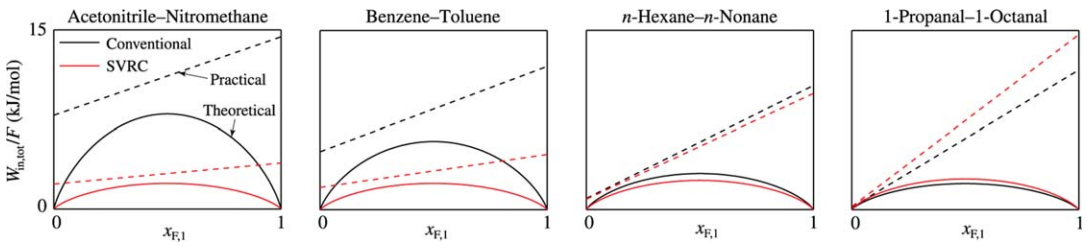

Figure 8. Comparison of minimum theoretical and minimum practical work inputs to the conventional and standard vapor recompression configurations for a sharp split as a function of mole fraction of the light component in the feed.

[Color figure can be viewed in the online issue, which is available at wileyonlinelibrary.com]

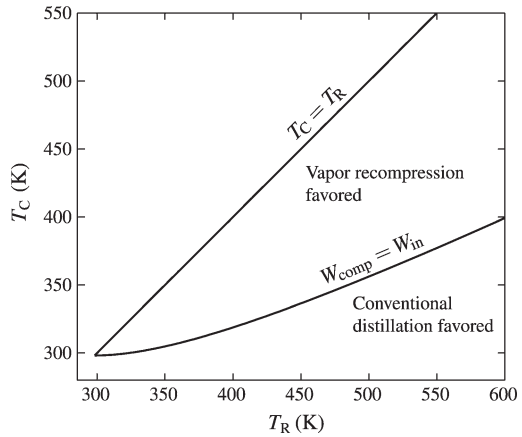

Figure 9. Plot of regions where vapor recompression is thermodynamically more efficient than conventional distillation as a function of T_C and T_R only.

Unfortunately, at least four variables need to be specified for a system: T_C, T_R, $\hat{C}_{p,1}^{IG}$, and λ, yet not all four can be represented independently on a two-dimensional plot. One way of overcoming this restriction is to use an approximation for λ in the form of the Trouton–Hildebrand–Everett rule,[66,67] which gives good estimates for nonpolar hydrocarbons

$$\frac{\lambda}{RT_C} = 4.0 + \ln(T_C/\mathrm{K}) \tag{24}$$

It can be shown, as has been done in Appendix A, that the minimum pressure ratio can be estimated using the following equation

$$\frac{P_{comp}}{P_0} = \exp\left([4.0 + \ln(T_C/\mathrm{K})]\left(1 - \frac{T_C}{T_R}\right)\right) \tag{25}$$

Equation 25 can be used to plot contours of specific P_{comp}/P_0 values in the $T_C - T_R$ space. These have been included in Figure 10. It is important to note that the practical compression ratios (say, $P_{comp}/P_0 < 3$) are almost entirely within the VRC region. The implication of this is that in almost all cases where VRC can practically be applied, that configuration is more efficient thermodynamically than conventional distillation.

Need for superheating of compressor inlet

It is also useful to determine whether or not superheating of the compressor inlet is required.

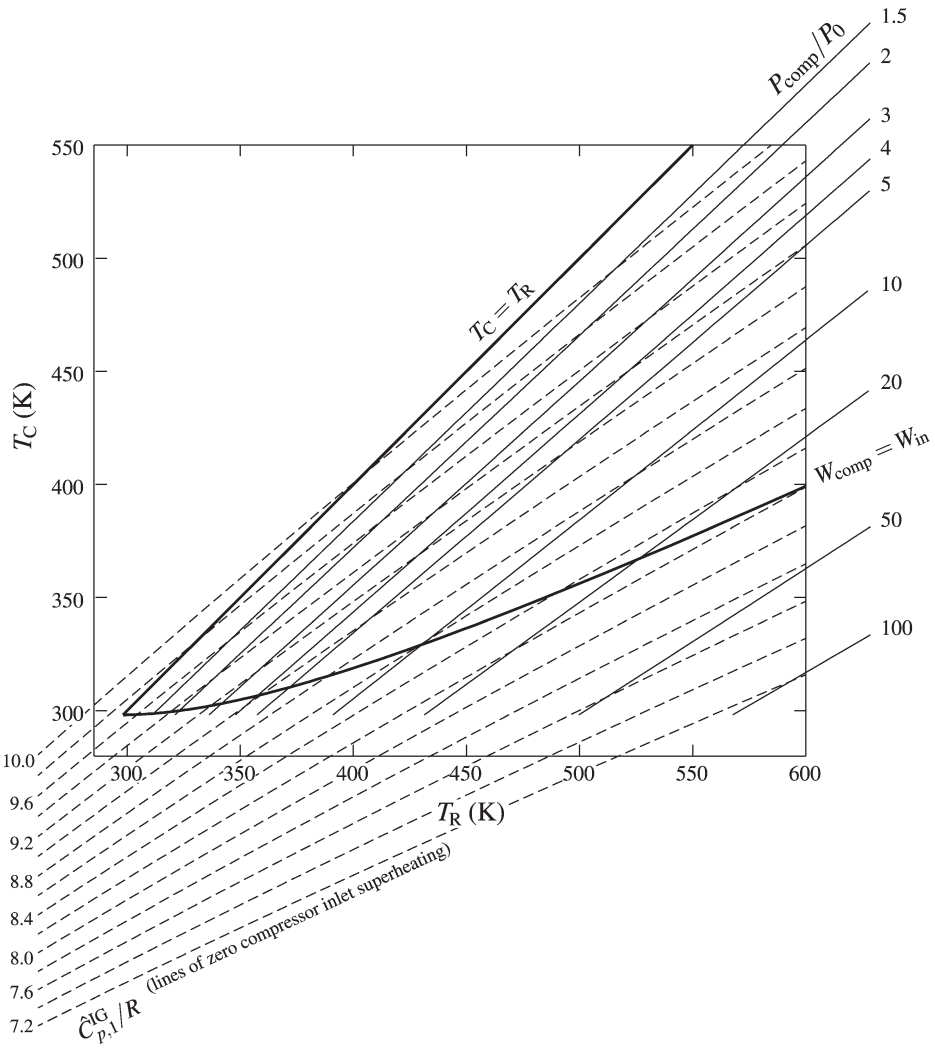

Figure 10. Plot of regions where vapor recompression is thermodynamically more efficient than conventional distillation as a function of T_C and T_R, with overlays of minimum required compression ratios, and lines of zero compressor inlet superheating for various $C_{p,1}^{IG}/R$ values.

The vapor enters the superheater at T_C and is heated to T_2, the expression for which is available in Appendix A. No superheating is required when $T_2 = T_C$. The equation for zero superheating is derived in Appendix A; the result is given here as

$$T_C = T_R \exp\left(\frac{R[4.0 + \ln(T_C/\mathrm{K})]}{\hat{C}_{p,1}^{IG}}\left(\frac{T_C}{T_R} - 1\right)\right) \quad (26)$$

For a specified value of $\hat{C}_{p,1}^{IG}/R$, Eq. 26 can be solved numerically to plot lines of zero superheating in the $T_C - T_R$ space, which have also been shown in Figure 10. This allows for rapid assessment of whether or not the inclusion of a superheater before the compressor is likely to be required, if the C_p^{IG} of the overhead vapor is known.

Interpretation of Figure 10

To use Figure 10, the $T_R - T_C$ coordinate is first located on the chart. If this point is within the VRC region (see Figure 9), it means that SVRC will likely be more thermodynamically efficient than conventional distillation for that system. However, even if it is thermodynamically favorable, it does not necessarily mean that SVRC can be practically implemented. To address this issue, the P_{comp}/P_0 ratio corresponding to the $T_R - T_C$ coordinate is located on the appropriate isobar on the chart. This value represents an estimate of the minimum pressure ratio that is required in the compressor; if this is lower than a practical maximum (around 3, as a guideline), then it is likely that the SVRC could be implemented practically, and rigorous simulation should be used to verify this estimate. Note that if the $T_R - T_C$ coordinate is close to the $W_{comp} = W_{in}$ line, and the pressure ratio is reasonable, rigorous simulation should be performed, as estimates using Figure 10 are likely to be inconclusive in this case.

The above decision process is summarized in the flowchart given in Figure 11.

Additionally, the $T_R - T_C$ coordinate will also have a $C_{p,1}^{IG}/R$ value associated with it, which is located on the appropriate dashed line. If the actual value of $C_{p,1}^{IG}/R$ is lower than the one corresponding to the $T_R - T_C$ coordinate, the vapor superheats on isentropic compression; otherwise, it partially condenses, and a superheater is required before to the compressor inlet. Although this is informative, it cannot provide information about the exact amount of superheating required; as such, it is not necessarily part of the decision-making process.

It should be reiterated that these are estimates only, because a number of simplifications must be made to arrive at this entirely graphical, generalized result. Consequently, it is used to assess whether SVRC is likely to be better than conventional distillation, and whether it could be implemented, but the result is not definitive.

Rigorous Simulation and Validation

The usefulness of Figure 10 is tested here by means of a number of examples, and validated using rigorous simulation in AspenTech's Aspen Plus. Figure 10 is intended only for rough, high-level estimates due to its numerous simplifying assumptions. The examples also serve to demonstrate how the results using Figure 10 should be interpreted.

Note that the compression ratio lines and the zero superheating lines are most accurate close to the $T_C = T_R$ line,

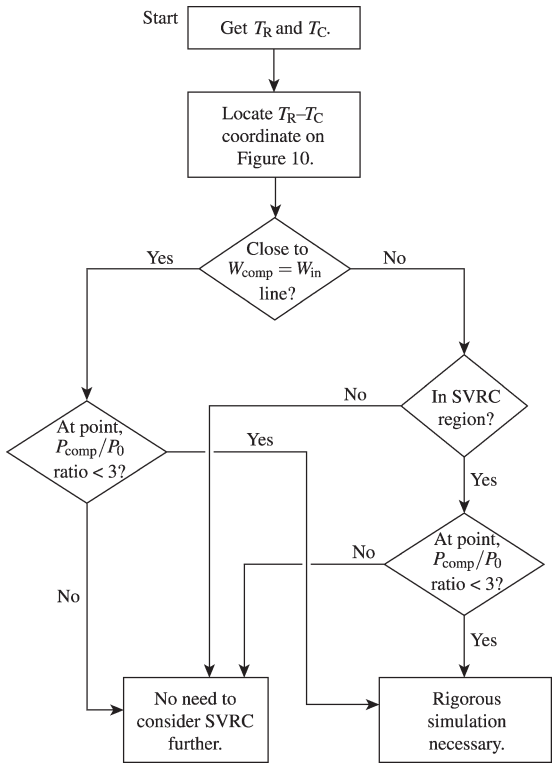

Figure 11. Flowchart representing the decision-making process with Figure 10.

because the constant properties assumed in the defining equations lose accuracy over wide temperature ranges. Additionally, the use of Eq. 24 makes the results less reliable when the light component is highly polar, for example, contains H-bonds. The examples here include systems that do not adhere to these restrictions.

The general connectivity of the simulated flow sheets is given for the conventional case in Figure 12, and in Figure 13 for the SVRC. The nonrandom two-liquid (NRTL) activity coefficient model was used for the vapor–liquid equilibrium calculations. The column was modeled using the RADFRAC block, and the compressor was modeled as completely isentropic.

For each example, the simulation settings are given in Appendix C.

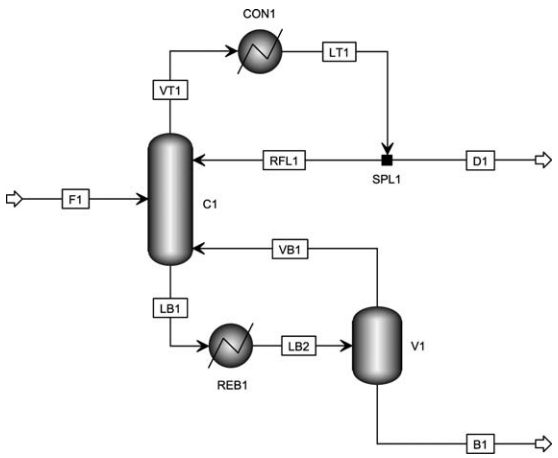

Figure 12. Aspen Plus flow sheet for the rigorous simulation of the conventional distillation column.

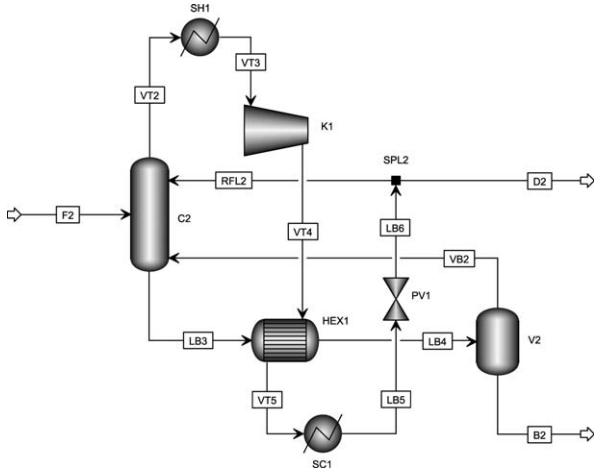

Figure 13. Aspen Plus flow sheet for the rigorous simulation of the standard vapor recompression configuration.

Design methodology

It is important to note that the purpose of these simulations was not to determine the optimal design, but rather to compare a conventional column with the SVRC, both of which have the same parameters (reflux ratio, product compositions, number of stages, feed stage, etc.). The design methodology for the Aspen Plus simulations was partially one of trial-and-error, using starting estimates for some of the key parameters.

The conventional column was simulated first. Once the feed and product compositions had been chosen, the Aspen Plus shortcut distillation model, DSTWU, was used to estimate the minimum reflux ratio $r_{\min}$. Thereafter, the reflux ratio was chosen as $r = 1.5\, r_{\min}$. Through simple mass balance, using this reflux ratio and the desired product compositions, the required split at SPL1, and the vapor fraction in REB1 (see Figure 12 for nomenclature) can be estimated. The column (C1) was simulated using the RADFRAC model, which initially had 10 stages. The feed stage was found to have little effect in these simulations, and was, thus, set to half-way up the column in each case, thereby eliminating a degree of freedom; had the optimal configuration been sought, greater care would have been taken regarding the feed stage. The simulation was run, and if—after some manual adjustment of the SPL1 and REB1 settings—the approximate product compositions were not achieved, the number of stages was increased, and the process repeated.

Once the conventional column had been simulated successfully, the SVRC simulation (as shown in Figure 13) was set up such that the RADFRAC column (C2) had exactly the same specification as in the conventional case. Similarly, SPL2 had the same split fraction as SPL1, and the cold stream outlet vapor fraction from HEX1 was the same as the vapor fraction in REB1. These parameters ensured that the column internals, and, thus, the product compositions, would be identical in both configurations. The compression ratio in K1 and the superheating in SH1 were estimated initially using a shortcut method,[65] and then adjusted simultaneously, until both were at a (rough) minimum which allowed the SVRC system to work, but resulted in no condensation in the compressor.

Example 1: 1-butene–n-butane

The normal boiling point of 1-butene is 266.91 K, and that of *n*-butane is 272.65 K, both of which are below the assumed ambient temperature of 298.15 K. To avoid the use of an external refrigeration system to remove heat at a sub-ambient temperature, it is simpler to run the system at a higher pressure, thereby raising the boiling points.

At a pressure of 400 kPa, 1-butene has a boiling point of 307.56 K, whereas *n*-butane has 315.09 K, both of which can readily be serviced using steam and cooling water. Consequently, the feed and column are set to this pressure. The average $\hat{C}_p^{\mathrm{IG}}$ of 1-butene at these two temperatures is 88.73 J/mol·K.

First, the point at $T_{\mathrm{R}} = 315.09\,\mathrm{K}$ and $T_{\mathrm{C}} = 307.56\,\mathrm{K}$ is located on Figure 10. This is well within the VRC zone, indicating that VRC should be thermodynamically preferable to conventional distillation for this split. The isobaric lines indicate that the minimum compression ratio of a bit less than 1.5—approximately 1.3—is required, which can be readily achieved in a compressor, meaning that VRC should be practically feasible. For this system, the value of $\hat{C}_p^{\mathrm{IG}}/R$ is 10.67. The point for this system lies between the zero superheating lines for $\hat{C}_p^{\mathrm{IG}}/R$ of 9.6 and 9.8. Because the actual $\hat{C}_p^{\mathrm{IG}}/R$ value of 10.67 is clearly higher than either of these, it is expected that superheating of the compressor inlet is required.

For the rigorous simulation, a feed of 1 kmol/h of a mixture with 63 mol % 1-butene and 37 mol % *n*-butane was sent into both columns, each with a reflux ratio of 14.38. The lowest compression ratio that could be used in the compressor successfully was 1.43, which was estimated reasonably well with Figure 10.

The simulation gave a distillate with $x_{\mathrm{D}} = (0.9989, 0.0011)$ and a bottoms with $x_{\mathrm{B}} = (0.0041, 0.9959)$.

For the conventional column, the only energy input is at the reboiler, which was found to have a load of 52.754 kW. From Eq. 1, the virtual work input associated with this heat can be estimated at 2.830 kW.

The SVRC had a work/energy input in the compressor of 2.597 kW, and a heat input in the superheater of 2.880 kW. The virtual work associated with the latter was estimated at 0.193 kW. The total energy input, therefore, was 5.477 kW, and the total work input was 2.790 kW.

The energy requirements of the SVRC were approximately 10 times smaller than for the conventional distillation column, with slightly lower overall work input, the latter being crudely approximated.

Example 2: hydrogen cyanide–acrylonitrile

There is a small region in Figure 10 where the compression ratio is practically implementable, but is in the region expected to be thermodynamically unfavorable with VRC. This example is intended to determine whether this is indeed the case.

Hydrogen cyanide has a normal boiling point of 298.85 K, whereas that of acrylonitrile is 350.50 K.

At this $T_{\mathrm{R}} - T_{\mathrm{C}}$ coordinate on Figure 10, the required compression ratio is at least 4, which is relatively high, although it may be possible to achieve the necessary compression in a single-case compressor. As aforementioned, this system was chosen to lie in the region where VRC is unfavorable.

For hydrogen cyanide at its boiling point, $\hat{C}_p^{\mathrm{IG}}/R = 4.309$. The zero superheating line corresponding to the coordinate for this system is at a value of approximately $\hat{C}_p^{\mathrm{IG}}/R = 9.0$;

because the actual value is significantly lower, it is highly unlikely that compressor inlet superheating is required.

The rigorous simulation was performed with a feed of 1 kmol/h having a composition of 71 mol % hydrogen cyanide and the balance acrylonitrile. The entire system was isobaric at 100 kPa. The minimum compression ratio was found to be 6.42, which is not lower than the estimated minimum. Moreover, as estimated, compressor superheating was not necessary.

In both configurations, the reflux ratio was set to 0.46, resulting in product compositions of $x_D = (0.9996, 0.0004)$ and $x_B = (0.0001, 0.9999)$.

In the conventional column, the heat input was 8.140 kW (associated virtual work input: 1.213 kW). The SVRC had work/energy input of 1.649 kW. Consequently, although the SVRC has lower energy requirements, its work input is higher than the conventional column's, as predicted with Figure 10.

Example 3: 1-propanol–n-octane

This example deviates from three of the assumptions in Figure 10: first, it is highly nonideal and contains an azeotrope; second, the overhead vapor includes an H-bond, such that Eq. 24 is less accurate; and finally, the split is not sharp.

The normal boiling point of 1-propanol is 370.35 K, and that of *n*-octane is 398.83 K. The azeotrope—as predicted with NRTL—occurs at 74.37 mol % 1-propanol, and has a temperature of 367.10 K.

A feed of 1 kmol/h of 23 mol % 1-propanol and the balance *n*-octane is to be separated into >70 mol % 1-propanol in the distillate, and >90 mol % *n*-octane in the bottoms. Prior to simulation, the exact temperatures of the distillate and bottoms are unknown, such that some assumptions must be made about these temperatures; it will be assumed that the distillate is at the temperature of the azeotrope (367.10 K) and the bottoms is at the temperature of the heavy key component (398.83 K).

Using this $T_R - T_C$ coordinate on Figure 10, it is expected that SVRC should be more thermodynamically efficient than conventional distillation, and that the compression ratio should be at least 2.5, approximately. The mole fraction-weighted C_p^{IG}/R of the overhead vapor at 367.10 K is 15.97; the zero superheating $C_{p,1}^{IG}/R$ corresponding to the coordinate for this system is 9.4. As the actual value is higher, it is expected that superheating will be required.

The simulation was performed using a reflux ratio of 0.547 in both the SVRC configuration and the conventional distillation. The resulting distillate had a composition of $x_D = (0.7189, 0.2811)$ and $x_B = (0.0088, 0.9912)$.

In the conventional case, the heat input was 6.567 kW, which has an associated work input of 1.585 kW.

In the SVRC case, as predicted with Figure 10, superheating was required. Because a fair amount of superheating is required, and as the amount of superheating required is not independent of the compression ratio, the minimum compression ratio is not straightforward; indeed, an optimization could be performed to minimize the work input. (Optimization is not the objective here; all that needs to be shown is whether or not the SVRC can be designed to have lower work input than conventional distillation, as was estimated.) The superheater was set to heat the overhead vapor by 65 K; the corresponding compression ratio could be no lower than 2.6.

The heat duty of the superheater was 1.266 kW, with an associated virtual work input of 0.392 kW. The compressor had energy/work input of 0.471 kW. Thus, the total work input was 0.863 kW, which is approximately half of the work input in the conventional case.

The prediction with Figure 10 was again good, despite departures from its inherent assumptions.

Example 4: multicomponent system

The final example deviates from the base assumptions by having more than two components, and not performing a sharp split. The feed in this problem is a quaternary mixture of methanol, 2-propanol, 2,6,8-trimethyl-4-nonanone, 1-undecanal with a flow of 1 kmol/h, and composition $x_F = (0.13, 0.22, 0.24, 0.41)$.

A rigorous simulation of a conventional distillation column with a reflux ratio of 0.429 resulted in a distillate of $x_D = \left(0.371, 0.628, 7.4 \times 10^{-8}, 2.3 \times 10^{-10}\right)$, which has temperature 345.78 K, and bottoms $x_B = \left(6.7 \times 10^{-5}, 9.0 \times 10^{-4}, 0.369, 0.630\right)$ at temperature 497.64 K. The activity coefficients were modeled using UNIFAC.

The heat load obtained from the simulation is 15.431 kW, which has an associated virtual work input of 6.186 kW.

The question to be answered is whether this split would benefit from a VRC system, and if such a system could realistically be implemented. On Figure 10, the relevant point for this system is at $T_C = 345.78\,K$ and $T_R = 497.64\,K$. At this coordinate, the system is in the region where conventional distillation is more efficient, such that no gains are expected using VRC. Moreover, the minimum compression ratio is estimated at higher than 20, meaning that practical implementation is clearly not feasible.

A rigorous simulation of the SVRC was not possible without excessive settings (several hundred degrees of superheating and compression ratios in excess of 100). A comparison of work inputs in the two configurations was, thus, not possible; however, Figure 10 correctly identified that the minimum compression ratio was much too high for practical implementation of the SVRC scheme.

Conclusions

The rigorous simulation, and subsequent comparison, of conventional distillation and SVRC can be a time-consuming exercise; without knowing ahead of time if there is potential benefit to SVRC, this effort may be wasted. It is useful for the engineer to be able to gain insight into whether SVRC is a realistic candidate for a given separation problem prior to performing rigorous simulation. Previously, there were no general guidelines or rapid estimation methods for determining the potential applicability of SVRC available in the open scientific literature. The work in this article bridges this gap: a novel, consolidated graphical process synthesis tool was presented to estimate whether VRC is likely to be thermodynamically favorable to conventional distillation, and if so, whether it can be implemented practically. This tool requires minimal information, namely distillate and bottoms temperatures, and optionally the overhead vapor heat capacity. It is entirely calculation-free, which makes it particularly useful for first-pass estimates during conceptual design and process synthesis.

A thermodynamic analysis and comparison were conducted on conventional distillation columns and the SVRC configuration. When considering only the energy inputs to the systems, the energy requirements for VRC were found to

be significantly lower with narrow-boiling mixtures, and somewhat lower in much wider-boiling ones.

However, a more thermodynamically accurate comparison using work flows—rather than simply energy flows—revealed that the quality of heat has a marked impact on the true efficiency of the two configurations. The thermodynamic benefits of VRC were found to be less clear on this basis than when comparing energy loads directly.

A very simple quantitative description of the region where SVRC is thermodynamically favorable to conventional distillation was given in Figure 9 as a function of distillate and bottoms temperatures only. This chart serves as a generalized, graphical estimate of the region in which SVRC is thermodynamically preferred.

This chart also provides additional insight: the SVRC region is broad enough to include many systems which have not had VRC applied to them in practice. The reason for this breadth is that some key factors limit practical implementation of VRC, despite thermodynamic favorability. The most significant of these is the required compressor pressure ratio, which in practice should typically be less than about 3 or 4. A less significant factor is the need for superheating of the compressor to avoid condensation that many saturated vapors undergo on compression.

To address the first of these concerns, an overlay of estimated minimum compression ratio was added to Figure 9 to produce Figure 10. This shows that the region where the compression ratio is reasonable is almost entirely a subset of the SVRC-preferred region, resulting in a relatively narrow band on Figure 10. The implication of this is that in almost all cases where the compression ratio is low enough to be applied practically, VRC is thermodynamically favorable to conventional distillation.

If the ideal gas heat capacity of the overhead vapor is known, an estimate can be made as to whether compressor inlet superheating is required. Lines of zero superheating for various heat capacities are also overlaid on Figure 10 to estimate whether or not a superheater before the compressor is necessary to avoid condensation in the compressor.

The usefulness of the presented process synthesis tool was tested using a number of examples, each of which extended the application beyond the initial set of assumptions used in deriving Figure 10. These examples were validated using rigorous simulation with Aspen Plus.

Although the key technical issues have been dealt with in this article, one important practical consideration, which, unfortunately, cannot be easily generalized, and which has, thus, not been dealt with in this article, is the economic impact of VRC on the total capital expenditure. Specifically, the compressor tends to be an expensive piece of equipment, which benefits from the economy of scale. Thus, once the technical viability has been established, the economics surrounding its implementation must be considered on a case-by-case basis; these costs are harder to quantify in advance. However, as energy costs continue to rise, the benefits of resource savings will begin to outweigh the setbacks of higher capital costs.

Notation

Roman letters

B = bottoms flow rate, mol/s
$\hat{C}_{p,i}$ = specific heat capacity of component i, J/mol·K
D = distillate flow rate, mol/s
F = feed flow rate, mol/s
L = liquid flow rate, mol/s
P_0 = ambient pressure, 101 325 Pa
r = L / D, reflux ratio
$\hat{S}$ = entropy, J/mol·K
S_{gen} = entropy generation, W/K
T = temperature, K
T_0 = ambient temperature, 298.15 K
T_b = normal boiling point, K
V = vapor flow, mol/s
x_i = liquid mole fraction of component i

Greek letters

α = relative volatility of light component with respect to heavy component
$\Delta\hat{H}_{mix}$ = enthalpy of mixing, J/mol
$\Delta\hat{S}_{mix}$ = entropy of mixing, J/mol·K
λ = latent heat/enthalpy of vaporization, J/mol

Subscripts and superscripts

B = relating to the bottoms stream
comp = relating to the compressor
D = relating to the distillate stream
F = relating to the feed stream
heavy = relating to the heavy key component
hex = relating to a heat exchanger
IG = ideal gas
L = liquid
light = relating to the light key component
min = minimum

Literature Cited

1. Freshwater DC. Thermal economy in distillation. *Trans Inst Chem Eng*. 1951;29:149–160.
2. Flower JR, Jackson R. Energy requirements in the separation of mixtures by distillation. *Trans Inst Chem Eng*. 1964;42:T249–T258.
3. King CJ. *Separation Processes*. New York: McGraw-Hill, 1980.
4. Humphrey JL. *Separation processes*: playing a critical role. *Chem Eng Prog*. 1995;91:31–45.
5. Rév E, Emtir M, Szitkai Z, Mizsey P, Fonyó Z. Energy savings of integrated and coupled distillation systems. *Comp Chem Eng*. 2001;25:119–140.
6. Hernández-Gaona CG, Cárdenas JC, Segovia-Hernández JG, Hernández S, Rico-Ramírez V. Second law analysis of conventional and nonconventional distillation sequences. *Chem Biochem Eng Q*. 2005;19:235–241.
7. Agrawal R. Synthesis of multicomponent distillation column configurations. *AIChE J*. 2003;49:379–401.
8. Caballero JA, Grossmann IE. Thermodynamically equivalent configurations for thermally coupled distillation. *AIChE J*. 2003;49:2864–2884.
9. Caballero JA, Grossmann IE. Synthesis of complex thermally coupled distillation systems including divided wall columns. *AIChE J*. In press. Available at: http://dx.doi.org/10.1002/aic.13912.
10. Shenvi AA, Shah VH, Agrawal R. New multicomponent distillation configurations with simultaneous heat and mass integration. *AIChE J*. 2013;59:272–282.
11. Petlyuk FB, Platonov VM, Slavinskii DM. Thermodynamically optimal method for separating multicomponent mixtures. *Int Chem Eng*. 1965;5:555–561.
12. Halvorsen IJ, Skogestad S. Shortcut analysis of optimal operation of petlyuk distillation. *Ind Eng Chem Res*. 2004;43:3994–3999.
13. Halvorsen IJ, Skogestad S. Energy efficient distillation. *J Nat Gas Sci Eng*. 2011;3:571–580.
14. Holland ST, Abbas R, Hildebrandt D, Glasser D. Complex column design by application of column profile map techniques: sharp-split petlyuk column. *Ind Eng Chem Res*. 2010;49:327–349.
15. Al-Elg AH, Palazoglu A. Modeling and control of a high-purity double-effect distillation column. *Comp Chem Eng*. 1989;13:1183–1187.
16. Agrawal R. Multieffect distillation for thermally coupled configurations. *AIChE J*. 2000;46:2211–2224.
17. Engelien HK, Skogestad S. Minimum energy diagrams for multieffect distillation arrangements. *AIChE J*. 2005;51:1714–1725.

18. Soave G, Feliu JA. Saving energy in distillation towers by feed splitting. *Appl Therm Eng*. 2002;22:889–896.
19. Holland ST. Column Profile Maps: A Tool for the Design and Analysis of Complex Distillation Systems. Ph.D. Thesis. University of the Witwatersrand. Johannesburg, South Africa, 2005.
20. Felbab N, Hildebrandt D, Glasser D. A new method of locating all pinch points in nonideal distillation systems, and its application to pinch point loci and distillation boundaries. *Comp Chem Eng*. 2011;35:1072–1087.
21. Fonyó Z. Thermodynamic analysis of rectification I. Reversible model of rectification. *Int Chem Eng*. 1974;14:18–7.
22. Le Goff P, Cachot T, Rivero R. Exergy analysis of distillation processes. *Chem Eng Technol*. 1996;19:478–485.
23. Fonyó Z, Benkő N. Comparison of various heat pump assisted distillation configurations. *Chem Eng Res Des*. 1998;76:348–360.
24. Nakaiwa M, Huang K, Naito K, Endo A, Owa M, Akiya T, Nakane T, Takamatsu T. A new configuration of ideal heat integrated distillation columns (HIDiC). *Comp Chem Eng*. 2000;24:239–245.
25. Olujić Ž, Fakhri F, de Rijke A, de Graauw J, Jansens PJ. Internal heat integration—the key to an energy-conserving distillation column. *J Chem Technol Biotechnol*. 2003;78:241–248.
26. Huang K, Matsuda K, Iwakabe K, Takamatsu T, Nakaiwa M. Interpreting design of an ideal heat-integrated distillation column through exergy analysis. *J Chem Eng Jpn*. 2006;39:963–970.
27. Huang K, Shan L, Zhu Q, Qian J. A totally heat-integrated distillation column (THIDiC) – the effect of feed pre-heating by distillate. *Appl Therm Eng*. 2008;28:856–864.
28. Mane A, Jana AK. A new intensified heat integration in distillation column. *Ind Eng Chem Res*. 2010;49:9534–9541.
29. Chen H, Huang K, Wang S. A novel simplified configuration for an ideal heat-integrated distillation column (ideal HIDiC). *Sep Purif Technol*. 2010;73:230–242.
30. Suphanit B. Optimal heat distribution in the internally heat-integrated distillation column (HIDiC). *Energy*. 2011;36:4171–4181.
31. Nakaiwa M, Huang K, Endo A, Ohmori T, Akiya T, Takamatsu T. Internally heat-integrated distillation columns: a review. *Chem Eng Res Des*. 2003;81:162–177.
32. Jana AK. Heat integrated distillation operation. *Appl Energy*. 2010;87:1477–1494.
33. Ferré JA, Castells F, Flores J. Optimization of a distillation column with a direct vapor recompression heat pump. *Ind Eng Chem Proc Des Dev*. 1985;24:128–132.
34. Mészáros I, Fonyó Z. Design strategy for heat pump assisted distillation system. *Heat Recov Syst*. 1986;6:469–476.
35. Annakou O, Mizsey P. Rigorous investigation of heat pump assisted distillation. *Heat Recov Syst CHP*. 1995;15:241–247.
36. Demirel Y. Thermodynamic analysis of separation systems. *Separ Sci Technol*. 2004;39:3897–3942.
37. Null HR. Heat pumps in distillation. *Chem Eng Prog*. 1976;72:58–64.
38. Mészáros I, Meili A. 1-Butene separation processes with heat pump assisted distillation. *Heat Recov Syst CHP*. 1994;14:315–322.
39. Quadri GP. Use heat pump for P–P splitter. Part 1: process design. *Hydrocarb Process*. 1981a;60:119–126.
40. Quadri GP. Use heat pump for P–P splitter. Part 2: process optimization. *Hydrocarb Process*. 1981b;60:147–151.
41. Carta R, Kovacic A, Tola G. Separation of ethylbenzene–xylenes mixtures by distillation: a possible application of the vapour recompression concept. *Chem Eng Commun*. 1982;19:157–165.
42. Omideyi T, Kasprzycki J, Watson F. The economics of heat pump assisted distillation systems–I. A design and economic model. *J Heat Recov Syst*. 1984;4:187–200.
43. Brousse E, Claudel B, Jallut C. Modelling and optimization of the steady state operation of a vapour recompression distillation column. *Chem Eng Sci*. 1985;40:2073–2078.
44. Flores J, Castells F, Ferré JA. Recompression saves energy. *Hydrocarb Process*. 1984;63:59–62.
45. Meili A, Stuecheli A. Distillation columns with direct vapor recompression. *Chem Eng*. 1987;94:133–143.
46. Muhrer CA, Collura MA, Luyben WL. Control of vapor recompression distillation columns. *Ind Eng Chem Res*. 1990;29:59–71.
47. Cheng HC, Luyben WL. Heat-integrated distillation columns for ternary separations. *Ind Eng Chem Proc Des Dev*. 1985;24:707–713.
48. Fitzmorris RE, Mah RSH. Improving distillation column design using thermodynamic availability analysis. *AIChE J*. 1980;26:265–273.
49. Itoh J, Niida K, Shiroko K, Umeda T. Analysis of the available energy in a distillation system. *Int Chem Eng*. 1980;20:379–385.
50. Kaiser V, Gourlia JP. The ideal-column concept: applying exergy to distillation. *Chem Eng*. 1985;92:45–53.
51. Taprap R, Ishida M. Graphic exergy analysis of processes in distillation column by energy-utilization diagrams. *AIChE J*. 1996;42:1633–1641.
52. Kayihan F. Optimum distribution of heat load in distillation columns using intermediate condensers and reboilers. *AIChE Symp Ser*. 1980;192:1–5.
53. Henley EJ, Seader JD. *Equilibrium-Stage Separation Operations in Chemical Engineering*. New York: John Wiley & Sons, 1981.
54. Gomez-Munoz A, Seader JD. Synthesis of distillation trains by thermodynamic analysis. *Comp Chem Eng*. 1985;9:311–341.
55. Glinos K, Malone MF. Net work consumption in distillation—shortcut evaluation and applications to synthesis. *Comp Chem Eng*. 1989;13:295–305.
56. Skogestad S. *Chemical and Energy Process Engineering*. Florida: CRC Press, 2009.
57. Terranova BE, Westerberg AW. Temperature–heat diagrams for complex columns. 1. Intercooled/interheated distillation columns. *Ind Eng Chem Res*. 1989;28:1374–1379.
58. Chiang TP, Luyben WL. Comparison of energy consumption in five heat-integrated distillation configurations. *Ind Eng Chem Proc Des Dev*. 1983;22:175–179.
59. Mullins OC, Berry RS. Minimization of entropy production in distillation. *J Phys Chem*. 1984;88:723–728.
60. Smith R, Jobson M, Chen L, Farrokhpanah S. Heat integrated distillation system design. *Chem Eng Trans*. 2010;21:19–24.
61. Linnhoff B, Dunford H, Smith R. Heat integration of distillation columns into overall processes. *Chem Eng Sci*. 1983;38:1175–1188.
62. Underwood AJV. Fractional distillation of multicomponent mixtures. *Chem Eng Prog*. 1948;44:603–614.
63. Patwardhan VS. Condensation of saturated vapours on isentropic compression: a simple criterion. *Heat Recov Syst CHP*. 1987;7:395–399.
64. Gmehling J, Kolbe B, Kleiber M, Rarey J. *Chemical Thermodynamics for Process Simulation*. Weinheim: Wiley-VCH, 2012.
65. Felbab N. Condensation of saturated vapours on compression and estimation of minimum suction superheating. *Appl Therm Eng*. 2013;52:527–530.
66. Everett DH. 519. Some correlations between thermodynamic properties and the structure of liquids. *J Chem Soc*. 1960;2566–2573.
67. Nash LK. Trouton and the T–H–E Rule. *J Chem Educ*. 1984;61:981–984.
68. Branan C, editor. *Rules of Thumb for Chemical Engineers, 4th ed*. Houston: Gulf Professional Publishing, 2005.

Appendix A: Derivations

Minimum practical energy input in conventional columns

The easiest way of estimating minimum reflux for an ideal mixture is to use Underwood's method.[62] For the split of a binary, saturated liquid feed—with known relative volatility (α)—to pure components, minimum reflux using Underwood's method simplifies to the following[68]

$$r_{\min} = \frac{1}{x_{F,1}(\alpha - 1)} \tag{A1}$$

Using the mass balance of the column internals, with a saturated liquid feed and the CMO assumption, it can easily be shown that the vapor flow through the column is given by

$$V = D(r + 1) \tag{A2}$$

For sharp splits, $D = Fx_{F,1}$; using this fact and Eqs. A1 and A2, the minimum vapor flow in the column can be estimated

$$V_{\min} = F\left(\frac{1}{\alpha-1} + x_{F,1}\right) \tag{A3}$$

The minimum practical heat input at the reboiler can be calculated as follows

$$Q_{\text{in, min}} = \lambda V_{\min} \tag{A4}$$

$$Q_{\text{in,min}} = F\lambda\left(\frac{1}{\alpha-1} + x_{F,1}\right) \tag{A5}$$

Minimum practical energy input in SVRC

The stream numbers used here are given in Figure 4.

The modifications that SVRC makes to the conventional configuration are external to the column itself; for the same split of the same feed, the internal specifications of the column can remain identical. Consequently, the SVRC has the same minimum vapor flow as the conventional configuration, given in Eq. A3.

The energy input into the compressor is found with an energy balance

$$W_{\text{comp, min}} = V_{\min}\hat{C}_{p,1}^{\text{IG}}(T_3 - T_2) \tag{A6}$$

The use of the superheater and the temperatures T_2 and T_3 depend on the fluid being compressed. The isentropic compression of an ideal gas is given by

$$\frac{P_{\text{comp}}}{P_0} = \left(\frac{T_3}{T_2}\right)^{\hat{C}_{p,1}^{\text{IG}}/R} \tag{A7}$$

If the saturated vapor superheats on compression, then $T_1 = T_2 = T_C$. Assuming isentropic compression, and constant λ (to use the Clausius–Clapeyron equation), the minimum T_3 can easily be deduced

$$T_3 = T_C \exp\left(\frac{\lambda}{\hat{C}_{p,1}^{\text{IG}}}\left(\frac{1}{T_C} - \frac{1}{T_R}\right)\right) \tag{A8}$$

Consequently, the energy input into the system is given by the compression of the vapor from T_3 to T_2 only, as $Q_{\text{sh}} = 0\,\text{W}$. Therefore, from Eqs. A3, A6, and A8

$$W_{\text{comp, min}} = F\hat{C}_{p,1}^{\text{IG}} T_C\left(\frac{1}{\alpha-1} + x_{F,1}\right)\left(\exp\left(\frac{\lambda}{\hat{C}_{p,1}^{\text{IG}}}\left(\frac{1}{T_C} - \frac{1}{T_R}\right)\right) - 1\right) \tag{A9}$$

The energy (and work) input into the system in this case is simply equal to $W_{\text{comp, min}}$.

If the saturated vapor condenses, then $T_1 = T_C$ and $T_3 = T_R$, while T_2 is given by

$$T_2 = T_R \exp\left(\frac{\lambda}{\hat{C}_{p,1}^{\text{IG}}}\left(\frac{1}{T_R} - \frac{1}{T_C}\right)\right) \tag{A10}$$

In this case, the energy input into the system is the sum of $Q_{\text{sh, min}}$ and $W_{\text{comp, min}}$. The superheater's duty, using Eqs. A3 and A10, is given by

$$Q_{\text{sh, min}} = F\hat{C}_{p,1}^{\text{IG}}\left(\frac{1}{\alpha-1} + x_{F,1}\right)\left(T_R \exp\left(\frac{\lambda}{\hat{C}_{p,1}^{\text{IG}}}\left(\frac{1}{T_R} - \frac{1}{T_C}\right)\right) - T_C\right) \tag{A11}$$

From Eqs. A3, A6, and A10, the energy input into the compressor is

$$W_{\text{comp, min}} = F\hat{C}_{p,1}^{\text{IG}} T_R\left(\frac{1}{\alpha-1} + x_{F,1}\right)\left(1 - \exp\left(\frac{\lambda}{\hat{C}_{p,1}^{\text{IG}}}\left(\frac{1}{T_R} - \frac{1}{T_C}\right)\right)\right) \tag{A12}$$

Compression ratio

If the overhead vapor is superheated on isentropic compression, the process is expressed as follows

$$\frac{P_{\text{comp}}}{P_0} = \left(\frac{T_3}{T_C}\right)^{\hat{C}_{p,1}^{\text{IG}}/R} \tag{A13}$$

The expression for T_3 is given in Eq. A8. Substituting this, along with Eq. 24, into Eq. A13 ultimately gives

$$\frac{P_{\text{comp}}}{P_0} = \exp\left([4.0 + \ln(T_C/\text{K})]\left(1 - \frac{T_C}{T_R}\right)\right) \tag{A14}$$

If the overhead vapor condenses on isentropic compression, the relationship between compression ratio and temperature is as follows

$$\frac{P_{\text{comp}}}{P_0} = \left(\frac{T_R}{T_2}\right)^{\hat{C}_{p,1}^{\text{IG}}/R} \tag{A15}$$

T_2 is given in Eq. A10. Again, if this is substituted into Eq. A15 and used along with Eq. 24, the compression ratio can be calculated as follows

$$\frac{P_{\text{comp}}}{P_0} = \exp\left([4.0 + \ln(T_C/\text{K})]\left(1 - \frac{T_C}{T_R}\right)\right) \tag{A16}$$

It should be no surprise that Eqs. A14 and A16 are identical; Figure 6 illustrates why the compression ratio must be the same in both cases.

Zero superheating of compressor inlet

The vapor enters the superheater at T_C and is heated to T_2, which is given in Eq. A10. No superheating is required when $T_2 = T_C$. From Eq. A10, the following can be deduced

$$T_C = T_R \exp\left(\frac{\lambda}{\hat{C}_{p,1}^{\text{IG}}}\left(\frac{1}{T_R} - \frac{1}{T_C}\right)\right) \tag{A17}$$

With the use of Eq. 24 in Eq. A17, the following is obtained

$$T_C = T_R \exp\left(\frac{R[4.0 + \ln(T_C/K)]}{\hat{C}_{p,1}^{IG}}\left(\frac{T_C}{T_R} - 1\right)\right) \quad \text{(A18)}$$

Appendix B: Heat Pumps with External Working Fluid and Bottoms Flashing

Heat-pump-assisted distillation with an external working fluid (Figure 1c) and bottoms flashing (Figure 1d) can both be analyzed in the same way as SVRC, using the assumptions listed in the section "Simplifying Assumptions." In fact, both of these configurations reduce to the same problem, which is the same as SVRC, except with heat rejection at T_C, and not T_R. Energy is added in the compressor as W_{comp} and rejected as Q_{out} at T_C in the trim condensers.

As with SVRC, the energy balance simply reduces to $W_{comp} = Q_{out}$.

To assess the best theoretical performance, the systems are assumed to be reversible, such that $S_{gen} = 0\,W/K$. Similarly to Eq. 12, the entropy analysis then reduces to

$$F\Delta\hat{S}_{mix} = \frac{W_{comp}}{T_C} \quad \text{(B1)}$$

If, as was done with SVRC, Eq. 7 is equated to Eq. B1, the following result is obtained

$$\frac{W_{comp}}{W_{in}} = \frac{T_R - T_C}{T_R - T_0} \quad \text{(B2)}$$

The implication of this result is that these two configurations are always better than conventional distillation when the condenser temperature is higher than ambient temperature. (If it is subambient, then a heat pump is required to remove the energy from the column, and the analysis changes.) Therefore, it would appear that only practical issues, not fundamental thermodynamic ones, prevent the widespread implementation of these configurations.

Appendix C: Aspen Plus Simulation Settings

Example 1

The feeds in either case (F1 and F2) are at their bubble point, at a pressure of 400 kPa, with a total flow of 1 kmol/h, and a composition of 0.63 1-butene and 0.37 *n*-butane.

C1 and C2 are identical: they have no reboiler or condenser in the RADFRAC block (these are external). They have 100 stages, with feeds (F1 or F2, respectively) being fed on stage 50. RFL1 and RFL2 are added back on stage 1, and VB1 and VB2 are added on stage 100. The column is isobaric at 400 kPa.

CON1 has zero pressure drop, and cools the stream to its bubble point.

V1 and V2 have zero pressure drop and zero heat duty.

SH1 is set to effect a 12 K temperature increase, with no pressure drop.

K1 has isentropic and mechanical efficiencies of 100%, and a pressure ratio of 1.43.

SPL1 and SPL2 send fractionally 0.9350 of LT1 and LB6 to RFL1 and RFL2, respectively. This results in a reflux ratio of 14.38 in both cases.

REB1 is set to heat LB1 to a vapor fraction of 0.9625. Similarly, HEX 1 has its cold outlet stream vapor fraction set to 0.9625, and a minimum approach temperature of 5 K.

SC1 has a heat duty of −5442.8014 W.

PV1 reduces the pressure back to 400 kPa.

Example 2

The following settings were used in the simulation

F1/F2: 1 kmol/h; 100 kPa; bubble point temperature; composition: 0.71 hydrogen cyanide, 0.29 acrylonitrile.

C1/C2: 20 stages; no condenser; no reboiler; RFL1/RFL2 on stage 1; F1/F2 on stage 10; VB1/VB2 on stage 20; 100 kPa condenser pressure.

CON1: zero pressure drop; bubble point.

V1/V2: zero pressure drop; zero heat duty.

SH1: zero pressure drop; zero heat duty.

K1: pressure ratio 6.42; 100% isentropic and mechanical efficiency.

SPL1/SPL2: fractionally 0.3165 of LT1/LB6 sent to RFL1/RFL2.

REB1: zero pressure drop; vapor fraction 0.765.

HEX1: cold stream outlet vapor fraction 0.765; 5 K minimum temperature approach.

SC1: zero pressure drop; heat duty −1287.8069W.

PV1: 100 kPa outlet pressure.

Example 3

The following settings were used in the simulation

F1/F2: 1 kmol/h; 100 kPa; bubble point temperature; composition: 0.23 1-propanol, 0.77 *n*-octane.

C1/C2: 6 stages; no condenser; no reboiler; RFL1/RFL2 on stage 1; F1/F2 on stage 3; VB1/VB2 on stage 6; 100 kPa condenser pressure.

CON1: zero pressure drop; bubble point.

V1/V2: zero pressure drop; zero heat duty.

SH1: zero pressure drop; 65 K temperature change.

K1: pressure ratio 2.6; 100% isentropic and mechanical efficiency.

SPL1/SPL2: fractionally 0.3536 of LT1/LB6 sent to RFL1/RFL2.

REB1: zero pressure drop; vapor fraction 0.43.

HEX1: cold stream outlet vapor fraction 0.43; 5 K minimum temperature approach.

SC1: zero pressure drop; heat duty −513.51014W.

PV1: 100 kPa outlet pressure.

Example 4

The following settings were used in the simulation

F1: 1 kmol/h; 100 kPa; bubble point temperature; composition: 0.13 methanol, 0.22 2-propanol, 0.24 2,6,8-trimethyl-4-nonanone, 0.41 1-undecanal.

C1: 10 stages; no condenser; no reboiler; RFL1 on stage 1; F1 on stage 5; VB1 on stage 10; 100 kPa condenser pressure.

CON1: zero pressure drop; bubble point.

V1: zero pressure drop; zero heat duty.

SPL1: fractionally 0.3 of LT1 sent to RFL1.

REB1: zero pressure drop; vapor fraction 0.5.

Manuscript received Dec. 1, 2012, and revision received Jan. 28, 2013.